

Search for $B^+ \rightarrow K^+ \ell^+ \ell^-$ and $B^0 \rightarrow K^{*0} \ell^+ \ell^-$

The BABAR Collaboration

July 25, 2000

Abstract

Using a sample of 3.7×10^6 $\Upsilon(4S) \rightarrow B\bar{B}$ events collected with the BABAR detector at the PEP-II storage ring, we search for the electroweak penguin decays $B^+ \rightarrow K^+ e^+ e^-$, $B^+ \rightarrow K^+ \mu^+ \mu^-$, $B^0 \rightarrow K^{*0} e^+ e^-$, and $B^0 \rightarrow K^{*0} \mu^+ \mu^-$. We observe no significant signals for these modes and set preliminary 90% C.L. upper limits of

$$\begin{aligned}\mathcal{B}(B^+ \rightarrow K^+ e^+ e^-) &< 12.5 \times 10^{-6}, \\ \mathcal{B}(B^+ \rightarrow K^+ \mu^+ \mu^-) &< 8.3 \times 10^{-6}, \\ \mathcal{B}(B^0 \rightarrow K^{*0} e^+ e^-) &< 24.1 \times 10^{-6}, \\ \mathcal{B}(B^0 \rightarrow K^{*0} \mu^+ \mu^-) &< 24.5 \times 10^{-6}.\end{aligned}$$

The BABAR Collaboration

B. Aubert, A. Boucham, D. Boutigny, I. De Bonis, J. Favier, J.-M. Gaillard, F. Galeazzi, A. Jeremie,
Y. Karyotakis, J. P. Lees, P. Robbe, V. Tisserand, K. Zachariadou

Lab de Phys. des Particules, F-74941 Annecy-le-Vieux, CEDEX, France

A. Palano

Università di Bari, Dipartimento di Fisica and INFN, I-70126 Bari, Italy

G. P. Chen, J. C. Chen, N. D. Qi, G. Rong, P. Wang, Y. S. Zhu

Institute of High Energy Physics, Beijing 100039, China

G. Eigen, P. L. Reinertsen, B. Stugu

University of Bergen, Inst. of Physics, N-5007 Bergen, Norway

B. Abbott, G. S. Abrams, A. W. Borgland, A. B. Breon, D. N. Brown, J. Button-Shafer, R. N. Cahn,
A. R. Clark, Q. Fan, M. S. Gill, S. J. Gowdy, Y. Groysman, R. G. Jacobsen, R. W. Kadel, J. Kadyk,
L. T. Kerth, S. Kluth, J. F. Kral, C. Leclerc, M. E. Levi, T. Liu, G. Lynch, A. B. Meyer, M. Momayezi,
P. J. Oddone, A. Perazzo, M. Pripstein, N. A. Roe, A. Romosan, M. T. Ronan, V. G. Shelkov, P. Strother,
A. V. Telnov, W. A. Wenzel

Lawrence Berkeley National Lab, Berkeley, CA 94720, USA

P. G. Bright-Thomas, T. J. Champion, C. M. Hawkes, A. Kirk, S. W. O'Neale, A. T. Watson, N. K. Watson

University of Birmingham, Birmingham, B15 2TT, UK

T. Deppermann, H. Koch, J. Krug, M. Kunze, B. Lewandowski, K. Peters, H. Schmuecker, M. Steinke

Ruhr Universität Bochum, Inst. f. Experimentalphysik 1, D-44780 Bochum, Germany

J. C. Andress, N. Chevalier, P. J. Clark, N. Cottingham, N. De Groot, N. Dyce, B. Foster, A. Mass,
J. D. McFall, D. Wallom, F. F. Wilson

University of Bristol, Bristol BS8 1TL, UK

K. Abe, C. Hearty, T. S. Mattison, J. A. McKenna, D. Thiessen

University of British Columbia, Vancouver, BC, Canada V6T 1Z1

B. Camanzi, A. K. McKemey, J. Tinslay

Brunel University, Uxbridge, Middlesex UB8 3PH, UK

V. E. Blinov, A. D. Bukin, D. A. Bukin, A. R. Buzykaev, M. S. Dubrovin, V. B. Golubev,
V. N. Ivanchenko, A. A. Korol, E. A. Kravchenko, A. P. Onuchin, A. A. Salmikov, S. I. Serednyakov,
Yu. I. Skovpen, A. N. Yushkov

*Budker Institute of Nuclear Physics, Siberian Branch of Russian Academy of Science, Novosibirsk 630090,
Russia*

A. J. Lankford, M. Mandelkern, D. P. Stoker

University of California at Irvine, Irvine, CA 92697, USA

A. Ahsan, K. Arisaka, C. Buchanan, S. Chun

University of California at Los Angeles, Los Angeles, CA 90024, USA

J. G. Branson, R. Faccini,¹ D. B. MacFarlane, Sh. Rahatlou, G. Raven, V. Sharma
University of California at San Diego, La Jolla, CA 92093, USA

C. Campagnari, B. Dahmes, P. A. Hart, N. Kuznetsova, S. L. Levy, O. Long, A. Lu, J. D. Richman,
W. Verkerke, M. Witherell, S. Yellin
University of California at Santa Barbara, Santa Barbara, CA 93106, USA

J. Beringer, D. E. Dorfan, A. Eisner, A. Frey, A. A. Grillo, M. Grothe, C. A. Heusch, R. P. Johnson,
W. Kroeger, W. S. Lockman, T. Pulliam, H. Sadrozinski, T. Schalk, R. E. Schmitz, B. A. Schumm,
A. Seiden, M. Turri, D. C. Williams
University of California at Santa Cruz, Institute for Particle Physics, Santa Cruz, CA 95064, USA

E. Chen, G. P. Dubois-Felsmann, A. Dvoretzkii, D. G. Hitlin, Yu. G. Kolomensky, S. Metzler, J. Oyang,
F. C. Porter, A. Ryd, A. Samuel, M. Weaver, S. Yang, R. Y. Zhu
California Institute of Technology, Pasadena, CA 91125, USA

R. Aleksan, G. De Domenico, A. de Lesquen, S. Emery, A. Gaidot, S. F. Ganzhur, G. Hamel de
Monchenault, W. Kozanecki, M. Langer, G. W. London, B. Mayer, B. Serfass, G. Vasseur, C. Yeche,
M. Zito
Centre d'Etudes Nucléaires, Saclay, F-91191 Gif-sur-Yvette, France

S. Devmal, T. L. Geld, S. Jayatilleke, S. M. Jayatilleke, G. Mancinelli, B. T. Meadows, M. D. Sokoloff
University of Cincinnati, Cincinnati, OH 45221, USA

J. Blouw, J. L. Harton, M. Krishnamurthy, A. Soffer, W. H. Toki, R. J. Wilson, J. Zhang
Colorado State University, Fort Collins, CO 80523, USA

S. Fahey, W. T. Ford, F. Gaede, D. R. Johnson, A. K. Michael, U. Nauenberg, A. Olivas, H. Park,
P. Rankin, J. Roy, S. Sen, J. G. Smith, D. L. Wagner
University of Colorado, Boulder, CO 80309, USA

T. Brandt, J. Brose, G. Dahlinger, M. Dickopp, R. S. Dubitzky, M. L. Kocian, R. Müller-Pfefferkorn,
K. R. Schubert, R. Schwierz, B. Spaan, L. Wilden
Technische Universität Dresden, Inst. f. Kern- u. Teilchenphysik, D-01062 Dresden, Germany

L. Behr, D. Bernard, G. R. Bonneaud, F. Brochard, J. Cohen-Tanugi, S. Ferrag, E. Roussot, C. Thiebaut,
G. Vasileiadis, M. Verderi
Ecole Polytechnique, Lab de Physique Nucléaire H. E., F-91128 Palaiseau, France

A. Anjomshoaa, R. Bernet, F. Di Lodovico, F. Muheim, S. Playfer, J. E. Swain
University of Edinburgh, Edinburgh EH9 3JZ, UK

C. Bozzi, S. Dittongo, M. Folegani, L. Piemontese
Università di Ferrara, Dipartimento di Fisica and INFN, I-44100 Ferrara, Italy

E. Treadwell
Florida A&M University, Tallahassee, FL 32307, USA

¹ Jointly appointed with Università di Roma La Sapienza, Dipartimento di Fisica and INFN, I-00185 Roma, Italy

R. Baldini-Ferroli, A. Calcaterra, R. de Sangro, D. Falciari, G. Finocchiaro, P. Patteri, I. M. Peruzzi,²
M. Piccolo, A. Zallo

Laboratori Nazionali di Frascati dell'INFN, I-00044 Frascati, Italy

S. Bagnasco, A. Buzzo, R. Contri, G. Crosetti, P. Fabbriatore, S. Farinon, M. Lo Vetere, M. Macri,
M. R. Monge, R. Musenich, R. Parodi, S. Passaggio, F. C. Pastore, C. Patrignani, M. G. Pia, C. Priano,
E. Robutti, A. Santroni

Università di Genova, Dipartimento di Fisica and INFN, I-16146 Genova, Italy

J. Cochran, H. B. Crawley, P.-A. Fischer, J. Lamsa, W. T. Meyer, E. I. Rosenberg
Iowa State University, Ames, IA 50011-3160, USA

R. Bartoldus, T. Dignan, R. Hamilton, U. Mallik
University of Iowa, Iowa City, IA 52242, USA

C. Angelini, G. Batignani, S. Bettarini, M. Bondioli, M. Carpinelli, F. Forti, M. A. Giorgi, A. Lusiani,
M. Morganti, E. Paoloni, M. Rama, G. Rizzo, F. Sandrelli, G. Simi, G. Triggiani

Università di Pisa, Scuola Normale Superiore, and INFN, I-56010 Pisa, Italy

M. Benkebil, G. Grosdidier, C. Hast, A. Hoecker, V. LePeltier, A. M. Lutz, S. Plaszczynski, M. H. Schune,
S. Trincaz-Duvoid, A. Valassi, G. Wormser

LAL, F-91898 ORSAY Cedex, France

R. M. Bionta, V. Brigljević, O. Fackler, D. Fujino, D. J. Lange, M. Mugge, X. Shi, T. J. Wenaus,
D. M. Wright, C. R. Wuest

Lawrence Livermore National Laboratory, Livermore, CA 94550, USA

M. Carroll, J. R. Fry, E. Gabathuler, R. Gamet, M. George, M. Kay, S. McMahon, T. R. McMahon,
D. J. Payne, C. Touramanis

University of Liverpool, Liverpool L69 3BX, UK

M. L. Aspinwall, P. D. Dauncey, I. Eschrich, N. J. W. Gunawardane, R. Martin, J. A. Nash, P. Sanders,
D. Smith

University of London, Imperial College, London, SW7 2BW, UK

D. E. Azzopardi, J. J. Back, P. Dixon, P. F. Harrison, P. B. Vidal, M. I. Williams

University of London, Queen Mary and Westfield College, London, E1 4NS, UK

G. Cowan, M. G. Green, A. Kurup, P. McGrath, I. Scott

University of London, Royal Holloway and Bedford New College, Egham, Surrey TW20 0EX, UK

D. Brown, C. L. Davis, Y. Li, J. Pavlovich, A. Trunov

University of Louisville, Louisville, KY 40292, USA

J. Allison, R. J. Barlow, J. T. Boyd, J. Fullwood, A. Khan, G. D. Lafferty, N. Savvas, E. T. Simopoulos,
R. J. Thompson, J. H. Weatherall

University of Manchester, Manchester M13 9PL, UK

² Jointly appointed with Univ. di Perugia, I-06100 Perugia, Italy

C. Dallapiccola, A. Farbin, A. Jawahery, V. Lillard, J. Olsen, D. A. Roberts

University of Maryland, College Park, MD 20742, USA

B. Brau, R. Cowan, F. Taylor, R. K. Yamamoto

Massachusetts Institute of Technology, Lab for Nuclear Science, Cambridge, MA 02139, USA

G. Blaylock, K. T. Flood, S. S. Hertzbach, R. Kofler, C. S. Lin, S. Willocq, J. Wittlin

University of Massachusetts, Amherst, MA 01003, USA

P. Bloom, D. I. Britton, M. Milek, P. M. Patel, J. Trischuk

McGill University, Montreal, PQ, Canada H3A 2T8

F. Lanni, F. Palombo

Università di Milano, Dipartimento di Fisica and INFN, I-20133 Milano, Italy

J. M. Bauer, M. Booke, L. Cremaldi, R. Kroeger, J. Reidy, D. Sanders, D. J. Summers

University of Mississippi, University, MS 38677, USA

J. F. Arguin, J. P. Martin, J. Y. Nief, R. Seitz, P. Taras, A. Woch, V. Zacek

Université de Montreal, Lab. Rene J. A. Levesque, Montreal, QC, Canada, H3C 3J7

H. Nicholson, C. S. Sutton

Mount Holyoke College, South Hadley, MA 01075, USA

N. Cavallo, G. De Nardo, F. Fabozzi, C. Gatto, L. Lista, D. Piccolo, C. Sciacca

Università di Napoli Federico II, Dipartimento di Scienze Fisiche and INFN, I-80126 Napoli, Italy

M. Falbo

Northern Kentucky University, Highland Heights, KY 41076, USA

J. M. LoSecco

University of Notre Dame, Notre Dame, IN 46556, USA

J. R. G. Alsmiller, T. A. Gabriel, T. Handler

Oak Ridge National Laboratory, Oak Ridge, TN 37831, USA

F. Colecchia, F. Dal Corso, G. Michelon, M. Morandin, M. Posocco, R. Stroili, E. Torassa, C. Voci

Università di Padova, Dipartimento di Fisica and INFN, I-35131 Padova, Italy

M. Benayoun, H. Briand, J. Chauveau, P. David, C. De la Vaissière, L. Del Buono, O. Hamon, F. Le

Diberder, Ph. Leruste, J. Lory, F. Martinez-Vidal, L. Roos, J. Stark, S. Versillé

Universités Paris VI et VII, Lab de Physique Nucléaire H. E., F-75252 Paris, Cedex 05, France

P. F. Manfredi, V. Re, V. Speziali

Università di Pavia, Dipartimento di Elettronica and INFN, I-27100 Pavia, Italy

E. D. Frank, L. Gladney, Q. H. Guo, J. H. Panetta

University of Pennsylvania, Philadelphia, PA 19104, USA

M. Haire, D. Judd, K. Paick, L. Turnbull, D. E. Wagoner

Prairie View A&M University, Prairie View, TX 77446, USA

J. Albert, C. Bula, M. H. Kelsey, C. Lu, K. T. McDonald, V. Miftakov, S. F. Schaffner, A. J. S. Smith,
A. Tumanov, E. W. Varnes

Princeton University, Princeton, NJ 08544, USA

G. Cavoto, F. Ferrarotto, F. Ferroni, K. Fratini, E. Lamanna, E. Leonardi, M. A. Mazzoni, S. Morganti,
G. Piredda, F. Safai Tehrani, M. Serra

Università di Roma La Sapienza, Dipartimento di Fisica and INFN, I-00185 Roma, Italy

R. Waldi

Universität Rostock, D-18051 Rostock, Germany

P. F. Jacques, M. Kalelkar, R. J. Plano

Rutgers University, New Brunswick, NJ 08903, USA

T. Adye, U. Egede, B. Franek, N. I. Geddes, G. P. Gopal

Rutherford Appleton Laboratory, Chilton, Didcot, Oxon., OX11 0QX, UK

N. Coptý, M. V. Purohit, F. X. Yumiceva

University of South Carolina, Columbia, SC 29208, USA

I. Adam, P. L. Anthony, F. Anulli, D. Aston, K. Baird, E. Bloom, A. M. Boyarski, F. Bulos, G. Calderini,
M. R. Convery, D. P. Coupal, D. H. Coward, J. Dorfan, M. Doser, W. Dunwoodie, T. Glanzman,
G. L. Godfrey, P. Grosso, J. L. Hewett, T. Himel, M. E. Huffer, W. R. Innes, C. P. Jessop, P. Kim,
U. Langenegger, D. W. G. S. Leith, S. Luitz, V. Luth, H. L. Lynch, G. Manzin, H. Marsiske, S. Menke,
R. Messner, K. C. Moffeit, M. Morii, R. Mount, D. R. Muller, C. P. O'Grady, P. Paolucci, S. Petrak,
H. Quinn, B. N. Ratcliff, S. H. Robertson, L. S. Rochester, A. Roodman, T. Schietinger, R. H. Schindler,
J. Schwiening, G. Sciolla, V. V. Serbo, A. Snyder, A. Soha, S. M. Spanier, A. Stahl, D. Su, M. K. Sullivan,
M. Talby, H. A. Tanaka, J. Va'vra, S. R. Wagner, A. J. R. Weinstein, W. J. Wisniewski, C. C. Young

Stanford Linear Accelerator Center, Stanford, CA 94309, USA

P. R. Burchat, C. H. Cheng, D. Kirkby, T. I. Meyer, C. Roat

Stanford University, Stanford, CA 94305-4060, USA

A. De Silva, R. Henderson

TRIUMF, Vancouver, BC, Canada V6T 2A3

W. Bugg, H. Cohn, E. Hart, A. W. Weidemann

University of Tennessee, Knoxville, TN 37996, USA

T. Benninger, J. M. Izen, I. Kitayama, X. C. Lou, M. Turcotte

University of Texas at Dallas, Richardson, TX 75083, USA

F. Bianchi, M. Bona, B. Di Girolamo, D. Gamba, A. Smol, D. Zanin

Università di Torino, Dipartimento di Fisica Sperimentale and INFN, I-10125 Torino, Italy

L. Bosisio, G. Della Ricca, L. Lanceri, A. Pompili, P. Poropat, M. Prest, E. Vallazza, G. Vuagnin

Università di Trieste, Dipartimento di Fisica and INFN, I-34127 Trieste, Italy

R. S. Panvini

Vanderbilt University, Nashville, TN 37235, USA

C. M. Brown, P. D. Jackson, R. Kowalewski, J. M. Roney
University of Victoria, Victoria, BC, Canada V8W 3P6

H. R. Band, E. Charles, S. Dasu, P. Elmer, J. R. Johnson, J. Nielsen, W. Orejudos, Y. Pan, R. Prepost,
I. J. Scott, J. Walsh, S. L. Wu, Z. Yu, H. Zobernig
University of Wisconsin, Madison, WI 53706, USA

1 Introduction

The rare decays $B \rightarrow K\ell^+\ell^-$ and $B \rightarrow K^*\ell^+\ell^-$, where ℓ is either an electron or muon, are highly suppressed in the Standard Model and are expected to occur via electroweak penguin processes. The internal loops in such processes lead to a $b \rightarrow s$ transition via an effective flavor-changing neutral current interaction. Standard Model predictions for these decays are dependent to some extent on the modeling of the strong interactions in the hadronic $B \rightarrow K^{(*)}$ transition, but calculations indicate that $\mathcal{B}(B \rightarrow K\ell^+\ell^-) \approx 6 \times 10^{-7}$, while $\mathcal{B}(B \rightarrow K^*\ell^+\ell^-) \approx 2 \times 10^{-6}$ [1]. These processes provide a possible window into physics beyond the Standard Model, since new, heavy particles such as those predicted by SUSY models can also enter the loops, resulting in significant changes to both the decay rates and kinematic distributions [2].

Experimentally, the small expected rates make searches for these modes difficult. In addition, backgrounds from tree-level processes, such as $B \rightarrow J/\psi K^{(*)}$, with $J/\psi \rightarrow \ell^+\ell^-$, complicate the analyses. Searches from CDF [3] and CLEO [4] have so far yielded only upper limits, although in the case of $B \rightarrow K^*\mu^+\mu^-$ the limit is only about a factor of two above the Standard Model prediction.

In this paper, we report the results of a preliminary analysis to investigate the backgrounds and the ability of the *BABAR* detector to reject them. We have analyzed an on-resonance data sample of 3.2 fb^{-1} , representing about a third of the current *BABAR* $\Upsilon(4S)$ integrated luminosity.

As in many other searches for very rare decays, there are important issues that we face in designing event selection criteria in a manner that does not bias the determination of the signal yield, or, at worst, create a false apparent signal in a small statistics event sample. The main goal of our study is to test the performance of a “blind” analysis in which the event selection is optimized without use of the signal or sideband regions in the data. The events in these regions are therefore selected without bias, and the sidebands can be used for background estimation. The decays $B^+ \rightarrow J/\psi K^+$ and $B^0 \rightarrow J/\psi K^{*0}$, which have the same topology as the signal, provide a useful control sample to compare data with Monte Carlo simulation. These events can be used to validate the efficiencies predicted by the full *Geant321* Monte Carlo simulation. An additional control sample is provided by events with $K^{(*)}e^\pm\mu^\mp$ candidates. Such events monitor the level of combinatorial backgrounds present in the sample. This analysis provides a basis for extending the measurement to the much larger data samples that *BABAR* will obtain in the future. The 3.2 fb^{-1} data sample is comparable in size, however, to that used in an earlier CLEO analysis, and we are able to obtain results of comparable sensitivity for the $B^+ \rightarrow K^+\ell^+\ell^-$ modes.

We analyze four decay modes: $B^+ \rightarrow K^+e^+e^-$, $B^+ \rightarrow K^+\mu^+\mu^-$, $B^0 \rightarrow K^{*0}e^+e^-$, and $B^0 \rightarrow K^{*0}\mu^+\mu^-$. The K^{*0} is reconstructed in the $K^+\pi^-$ final state. In each case, we include the charge conjugate mode as well.

2 The *BABAR* detector and data sample

The *BABAR* detector is described in detail elsewhere [6]. All components of the detector are used for this study. Of particular importance for this analysis are the charged tracking system and the detectors used for particle identification. At radii between about 3 cm and 14 cm, charged tracks are measured with high precision in a five-layer silicon vertex tracker (SVT). This device comprises 52 modules built from double-sided AC-coupled silicon strip detectors. Tracking beyond the SVT is provided by the 40 layer drift chamber, which extends from 23.6 cm to 80.9 cm. Just outside the drift chamber is the DIRC, which is a Cherenkov ring-imaging particle identification system.

Cherenkov light is produced by charged tracks as they pass through an array of 144 five-meter-long fused silica quartz bars; the light is transmitted to the ends of the bars by total internal reflection, preserving the information on the angle of the light emission with respect to the track direction. Electrons are detected using an electromagnetic calorimeter comprising 6580 thallium-doped CsI crystals. Muons are detected in the Instrumented Flux Return (IFR), in which resistive plate chambers (RPCs) are interleaved with the iron plates of the flux return.

The data used in the analysis were collected with the *BABAR* detector at the PEP-II storage ring. We analyze a subsample of this data consisting of 3.2 fb^{-1} taken on the $\Upsilon(4S)$ resonance and 1.2 fb^{-1} at a slightly lower energy to obtain a pure continuum sample. For the purpose of optimizing the event selection, the following simulated event samples were used:

- 4.2 million generic $\Upsilon(4S) \rightarrow B\bar{B}$ events generated using the **Geant321** package,
- 4.2 million continuum $c\bar{c}$ events (**Geant321**),
- 4.8 million continuum $u\bar{u}$, $d\bar{d}$, and $s\bar{s}$ events (**Geant321**),
- 50 fb^{-1} of a fast, parametrized Monte Carlo simulation with the correct mixture of $B\bar{B}$ and continuum events,
- 5,000 events for each signal mode (**Geant321**).

3 Kinematic properties of signal events

The properties of $\Upsilon(4S) \rightarrow B\bar{B}$ events containing a $B \rightarrow K^{(*)}\ell^+\ell^-$ decay are modeled with a full **Geant321** Monte Carlo simulation using the event generator EvtGen [8]. We have implemented a generator based on the matrix elements computed in Ref. [1]. Although there are significant uncertainties due to strong interaction effects, the matrix elements can be rigorously parametrized in terms of form factors, which are Lorentz-invariant functions of $q^2 = M_{\ell^+\ell^-}^2$.

In the regions of q^2 near the J/ψ and $\psi(2S)$ resonances, interference occurs between the penguin amplitude and that for charmonium production, since the J/ψ and $\psi(2S)$ can decay into $\ell^+\ell^-$. This interference enhances the rate on the low-mass side of the resonance and suppresses it on the high side. These effects are modeled in Ref. [1], but not in our Monte Carlo generator. However, since $B \rightarrow J/\psi K^{(*)}$ and $B \rightarrow \psi(2S)K^{(*)}$ are major backgrounds in our analysis, we eliminate most of these mass regions, as described in the following section. Small residual interference effects are expected for masses close to our exclusion regions, but we have ignored these in the present study. Further enhancements in the rate, along with related interference effects, are expected from charmonium resonances with masses above the $\psi(2S)$. These effects are relatively small compared to the expected electroweak penguin contribution, and they are ignored in this study.

The Dalitz plot and q^2 distributions resulting from these matrix elements are shown in Fig. 1. For Dalitz plot variables we have chosen q^2 and E_{lep} , where the lepton energy is given in the B meson rest frame, and the positive lepton is selected for the case $B^+ \rightarrow K^+\ell^+\ell^-$ and $B^0 \rightarrow K^*\ell^+\ell^-$ (the negative lepton is selected for the charge-conjugate states). For $B \rightarrow K\ell^+\ell^-$, the q^2 distribution peaks at low values, corresponding to rapid K recoil in the B rest frame. For $B \rightarrow K^*\ell^+\ell^-$ the q^2 distribution peaks at large values, corresponding to slow K^* recoil in the B rest frame, but there is a pole in the amplitude at $q^2 = 0$, where the photon becomes real. The decay $B \rightarrow K\ell^+\ell^-$ does not have a pole at $q^2 = 0$ because $B \rightarrow K\gamma$ is forbidden by angular momentum conservation.

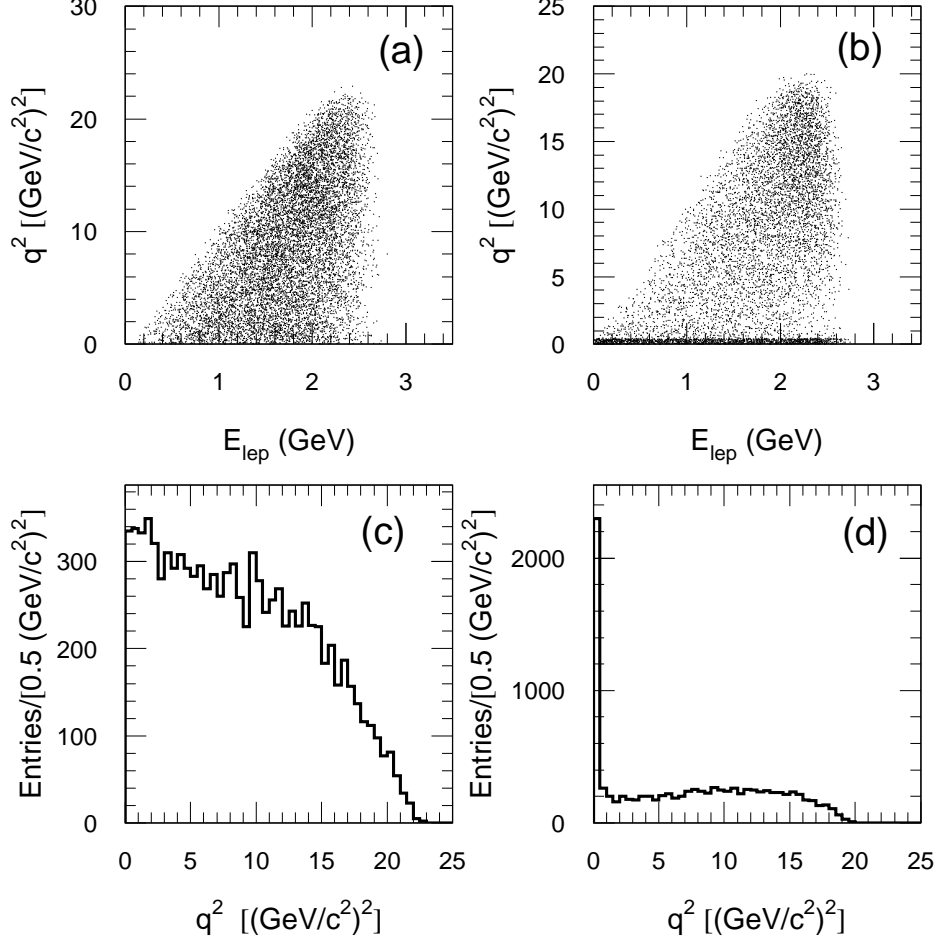


Figure 1: Monte Carlo simulated distributions for signal processes (a) Dalitz plot for $B \rightarrow Ke^+e^-$, (b) Dalitz plot for $B \rightarrow K^*e^+e^-$, (c) $q^2 = M_{e^+e^-}^2$ distribution for $B \rightarrow Ke^+e^-$, and (d) q^2 distribution for $B \rightarrow K^*e^+e^-$.

4 Overview of the analysis method

The analysis method exploits the strong signature and kinematic constraints for the $B \rightarrow K^{(*)}\ell^+\ell^-$ decay and the broad capabilities of the *BABAR* detector. Lepton and kaon identification, good momentum measurement, and the constraint associated with the known beam energies are essential for the search. Because even low-level backgrounds can be problematic, we have to be concerned about a possible “cocktail” of small contributions. Some of the most important sources are:

- $B \rightarrow J/\psi K^{(*)}$ or $B \rightarrow \psi(2S)K^{(*)}$ with J/ψ or $\psi(2S) \rightarrow \ell^+\ell^-$. If one of the leptons radiates a photon, the mass of the dilepton system can fall below the resonance veto region. These events must be rejected with high efficiency, since they have precisely the same topology as signal events.

- Combinatorial backgrounds from random leptons and kaons in $B\bar{B}$ and continuum processes ($e^+e^- \rightarrow q\bar{q}$, where $q = u, d, s, \text{ or } c$). In general, the lepton candidates arise from semileptonic decays, although leptons from photon conversions or from hadrons faking a lepton signature also contribute at a low level.
- Certain backgrounds can peak in the signal region, but these are quite rare and easily rejected. An example is $B^+ \rightarrow \bar{D}^0\pi^+$ with $\bar{D}^0 \rightarrow K^+\pi^-$. If both pions are misidentified as muons, this process can be confused with the signal. This type of three-body background is easily rejected with suitable reassignment of particle identification hypotheses and a veto on the D mass region.

Our goal in the present search is to gain an understanding of background levels and distributions and to set limits. For this purpose, we assume that each event in the signal region is potentially due to the signal process and do not perform a background subtraction. However, we do carry through a background estimation procedure using the sidebands in data and compare the results with those obtained by applying the procedure to the full `Geant321` simulation.

The signal region is defined as a rectangle in the plane defined by two kinematic variables, the beam-energy substituted mass of the B candidate m_{ES} , and the energy difference ΔE [6], where

$$m_{ES} = \sqrt{\left(\frac{\sqrt{s}}{2}\right)^2 - \left(\sum_{\alpha=1}^n \mathbf{p}_\alpha^*\right)^2},$$

$$\Delta E = \sum_{\alpha=1}^n \sqrt{m_\alpha^2 + |\mathbf{p}_\alpha^*|^2} - \sqrt{s}/2.$$

The index α is over the particles that make up the candidate B meson system. m_α are the masses of the particles and \mathbf{p}_α^* are their momenta measured in the $\Upsilon(4S)$ center of mass frame. $\sqrt{s}/2$ is one half of the center of mass energy. It is important to distinguish between the laboratory frame, in which the beams have energies $E_{e^-} \approx 9.0$ GeV and $E_{e^+} \approx 3.1$ GeV, and the center of mass frame, in which the beam energies are equal and the $\Upsilon(4S)$ is produced at rest. In a symmetric-energy machine, these frames are identical, but at PEP-II the center of mass frame is moving with respect to the laboratory with a boost factor $\beta\gamma \approx 0.56$.

5 Event selection

We select events with at least five good quality tracks, with 20 or more hits in the drift chamber and originating from the beam spot. Initially, we also require either two loosely identified, oppositely-charged electrons, muons, or an electron-muon pair (for combinatoric background studies). In addition, we require $R_2 < 0.8$, where R_2 is the ratio of the second and zeroth Fox-Wolfram moments [7]. This requirement provides a first suppression of continuum events, which have a more collimated (“jet-like”) event topology than $B\bar{B}$ events. At this stage, R_2 is evaluated in the center of mass frame using charged tracks only. Events passing these loose event selection criteria are further selected by requiring the electron and muon momenta in the lab frame to satisfy $p_e > 0.5$ GeV/ c and $p_\mu > 1.0$ GeV/ c . Electrons are identified on the basis of several quantities, primarily E/p_e , where E is the energy measured in the CsI electromagnetic calorimeter and p_e is the momentum determined by the tracking system. This ratio is near one for electrons or positrons. Muons are identified primarily by the number of interaction lengths of iron penetrated by the charged track

through the magnet flux return, which is instrumented with layers of resistive-plate chambers. The events are then required to lie within a large, rectangular region in the ΔE vs. m_{ES} plane: $m_{ES} > 5.0 \text{ GeV}/c^2$ and $|\Delta E| < 0.8 \text{ GeV}$.

After these basic event selection criteria, we apply a tighter set of particle identification requirements. In addition, electrons and positrons are required to pass the conversions veto, which suppresses the leptons that are likely to have come from photon conversions in the material. The kaon identification is based on combining the energy loss information (dE/dx) from the silicon vertex detector and the drift chamber for momenta $p < 0.6 \text{ GeV}/c$, with the knowledge of the Cherenkov angle from the DIRC for $p > 0.6 \text{ GeV}/c$. For the $B \rightarrow K\ell^+\ell^-$ modes we require that the kaon have $p_K > 0.6 \text{ GeV}/c$ in the lab frame.

For the $B^0 \rightarrow K^{*0}\ell^+\ell^-$ channels, we reconstruct the K^{*0} in the $K^+\pi^-$ final state. The kaon candidate is required to be identified as a kaon, while there are no particle identification requirements on the pion candidate. The mass of the $K^+\pi^-$ pair is required to be within $75 \text{ MeV}/c^2$ of the K^{*0} mass.

The next step is to veto $B \rightarrow J/\psi K^{(*)}$ and $B \rightarrow \psi(2S)K^{(*)}$. The requirements used for this purpose are somewhat complicated and are shown in Fig. 2. We remove events with dilepton masses consistent with those of the J/ψ or $\psi(2S)$. These veto regions are shown as pairs of vertical lines in the ΔE vs. $M_{\ell^+\ell^-}$ plane. However, bremsstrahlung or track mismeasurement can result in a large departure of the dilepton mass from the J/ψ or $\psi(2S)$ masses. Such departures are also accompanied by a shift in ΔE . We, therefore, remove these events by applying a correlated selection in this plane. Finally, a pair of horizontal lines is shown. There are veto regions above and below these lines, while the signal region lies between them. This region between the horizontal lines corresponds to the requirement that ΔE be consistent with zero. This requirement is not part of the charmonium veto *per se* but is still useful to see on this figure, because it further restricts the allowed region in this plane. Veto regions for the dimuon final state are defined in a similar way, but the definitions are somewhat different, since there is less bremsstrahlung. The $B \rightarrow J/\psi K$ modes can also pass this veto if the kaon is misidentified as a lepton (most often a muon). In a similar way $B \rightarrow D^0\pi$, where $D^0 \rightarrow K^-\pi^+$, can pass our selection criteria if both of the leptons are fake. These effects can be suppressed by re-assigning the particle masses and excluding mass combinations around the J/ψ and the D^0 .

Continuum background is suppressed by using a four-variable Fisher discriminant. The variables are the R_2 , which at this stage is computed using both charged and neutral candidates, the cosine of the angle between the B candidate and the z axis in the center of mass frame, the cosine of the angle between the thrust axis of the signal and that of the rest of the event in the center of mass frame, and the invariant mass of the kaon and the oppositely charged lepton. The last variable helps discriminate against the D semileptonic decays, as it will tend to be below the D mass. Both continuum and $B\bar{B}$ combinatorial background is further suppressed by requiring that the combined B vertex probability be greater than 0.1%.

Finally, we select the signal box in the ΔE vs. m_{ES} plane: $5.272 < m_{ES} < 5.286 \text{ GeV}$ (3σ) and $-0.10 < \Delta E < 0.06 \text{ GeV}$ ($|\Delta E| < 0.06 \text{ GeV}$) for the electron (muon) channels.

The net effect of our analysis selection criteria on the Dalitz plot is shown in Fig. 3. The requirements to remove $B \rightarrow J/\psi K$ and $B \rightarrow \psi(2S)K$ decays are evident as horizontal gaps, while those on the minimum lepton energy in the lab frame result in a loss of acceptance around the edges of the Dalitz plot.

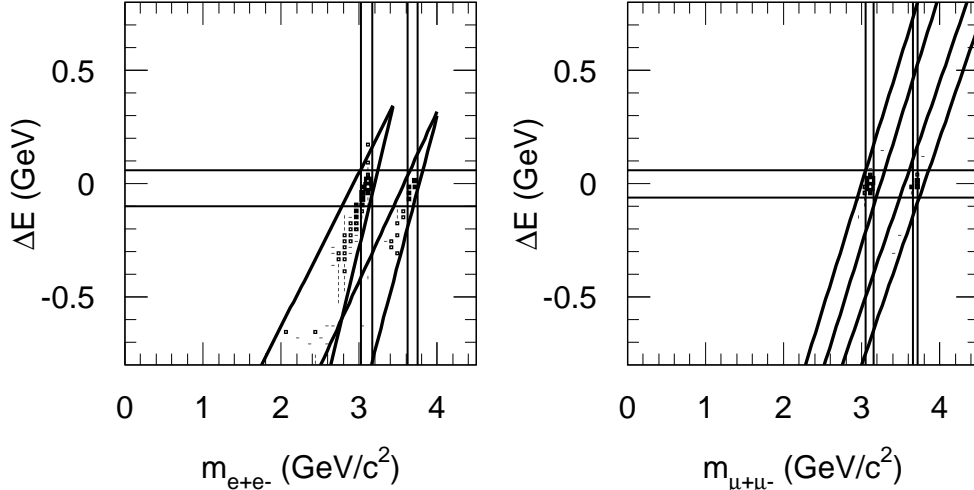


Figure 2: Regions in the ΔE vs. $M_{\ell+\ell^-}$ plane used to exclude $J/\psi K^{(*)}$ and $\psi(2S) K^{(*)}$ events: (a) shows the veto regions for the $J/\psi K^{(*)}$ and $\psi(2S) K^{(*)}$ events, where the J/ψ or $\psi(2S) \rightarrow e^+e^-$, (b) shows the veto regions for the $J/\psi K^{(*)}$ and $\psi(2S) K^{(*)}$ events, where the J/ψ or $\psi(2S) \rightarrow \mu^+\mu^-$. The regions between the close pairs of vertical lines correspond to the nominal J/ψ and $\psi(2S)$ resonance regions and are vetoed. The diagonal lines veto the events with bremsstrahlung and track mismeasurement. In the electron channel, the effects of bremsstrahlung are very substantial, which necessitates the use of triangular selection criteria. The signal region lies between the two horizontal lines except for the area excluded by the other vetos.

6 Physics results

Figure 4 shows a large ΔE vs. m_{ES} region (the “grand sideband”) and a small box indicating the signal region for each of the four modes. These scatter plots show a trend of decreasing background as ΔE increases from negative to positive values; this is a characteristic of $B\bar{B}$ background, where the energy of three or four randomly selected tracks is not as high as the nominal B energy in the center of mass frame. Events from the continuum have a more uniform distribution in ΔE and are more important for positive ΔE values.

Figure 5 shows the data distribution in m_{ES} after applying all other event selection criteria (including the requirement that the events lie within the ΔE signal region). The distributions are fit to the ARGUS function [5], whose shape is derived from the large statistics fast Monte Carlo simulation, and are used to estimate the background contribution to the m_{ES} signal region. For this study, however, we do not subtract this estimated background from the yield in the signal region; for the purpose of setting the limits we assume that all events in the signal region might be due to the signal events.

Table 1 lists the signal efficiencies, total yield, the expected background, and the 90% C.L. upper limits on the branching fractions. The signal efficiencies were determined from the signal Monte Carlo events. The efficiencies include the branching fractions for the K^{*0} modes. The table also lists the total systematic error, determined as described in Section 7. It is important to note that because we decided before the measurement that our result would be expressed as an upper limit, we do not need to apply the Feldman-Cousins procedure (Ref. [10]), for a two-sided confidence

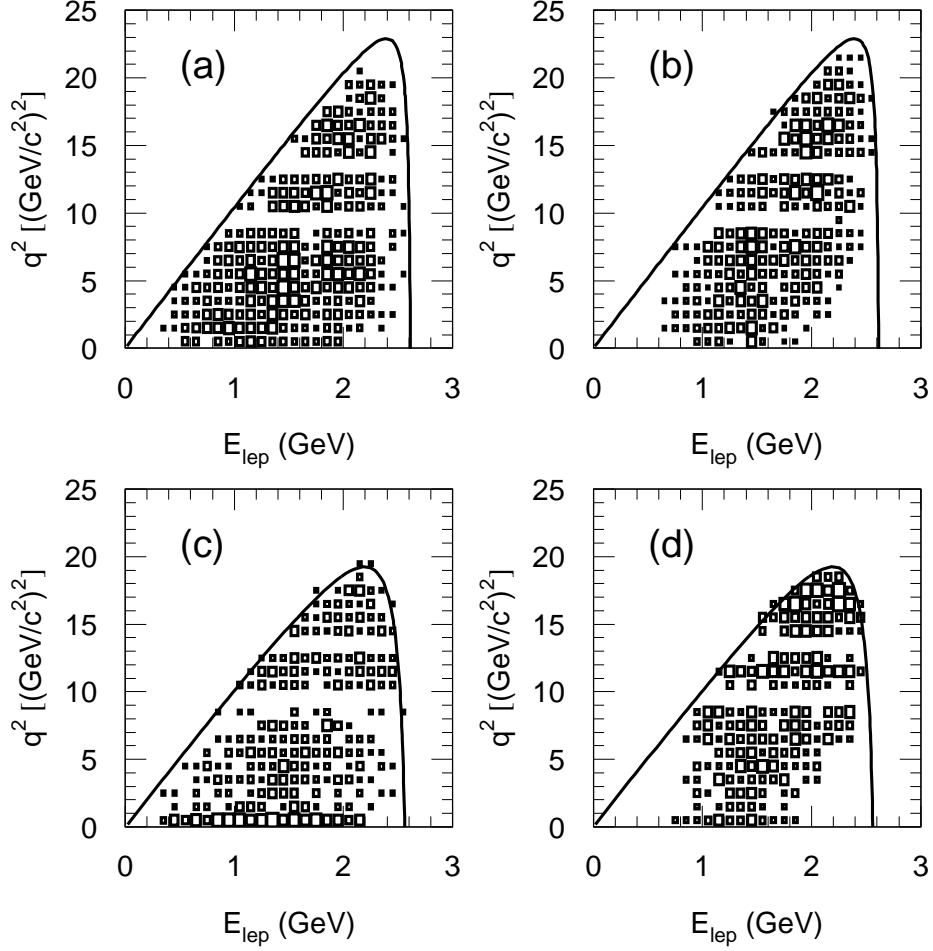


Figure 3: Effects of the charmonium veto requirements on the dilepton mass distributions for (a) $B^+ \rightarrow K^+ e^+ e^-$, (b) $B^+ \rightarrow K^+ \mu^+ \mu^-$, (c) $B^0 \rightarrow K^{*0} e^+ e^-$, and (d) $B^0 \rightarrow K^{*0} \mu^+ \mu^-$.

interval, but instead use the original procedure specified in the Particle Data Book [9], in which zero observed events corresponds to an upper limit of 2.3 events.

7 Systematic studies

As we are setting a conservative limit by assuming that all events observed in the signal region are in fact signal, the only systematic effects that affect the limits are those due to the modeling of our signal efficiency and the number of produced B mesons in our sample. Table 2 summarizes the systematic uncertainties that we have considered. The uncertainty on the tracking efficiency is 2.5% per track. Lepton and kaon identification efficiencies are measured in control samples in data (e.g., a Bhabha sample for electrons), where a measure of the uncertainty is obtained by

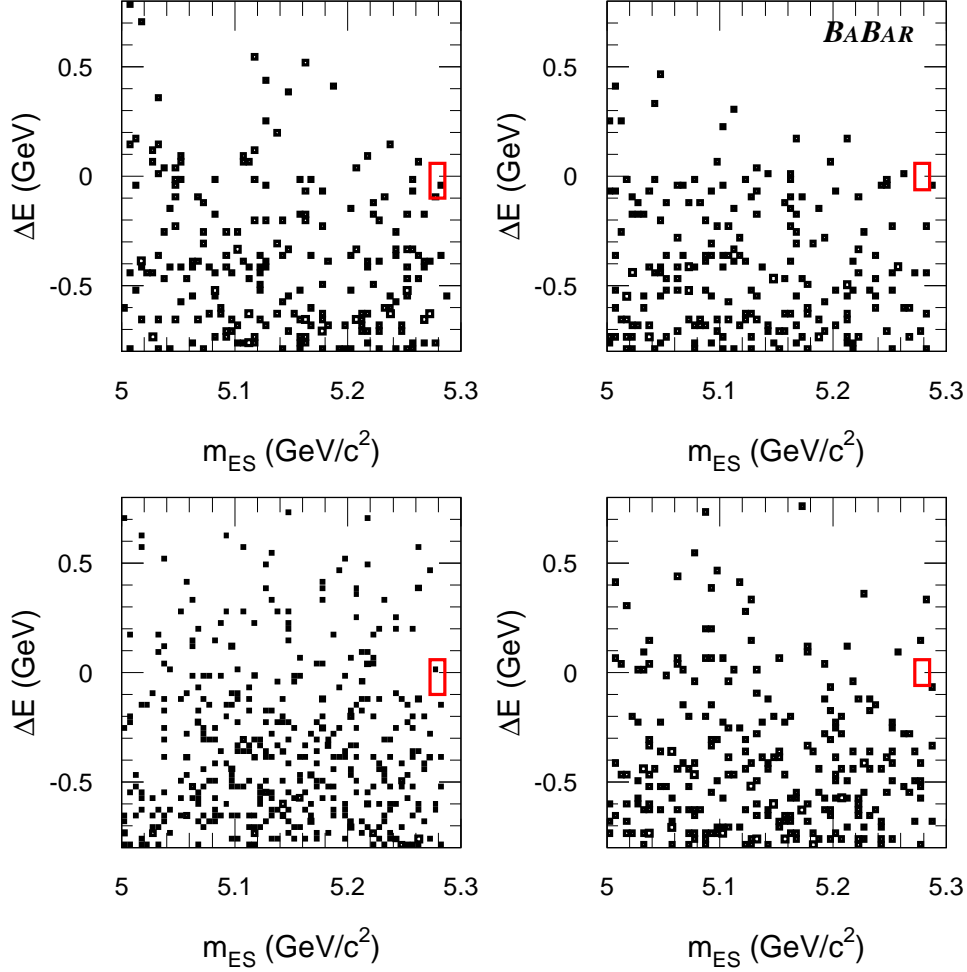


Figure 4: ΔE vs. m_{ES} (grand sideband) for data: (a) $B^+ \rightarrow K^+e^+e^-$, (b) $B^+ \rightarrow K^+\mu^+\mu^-$, (c) $B^0 \rightarrow K^{*0}e^+e^-$, and (d) $B^0 \rightarrow K^{*0}\mu^+\mu^-$. The smaller boxes show the signal region.

comparing different control samples. We assign an error of 2.0% per electron, 2.5% per muon, and 3.0% per kaon. We have also studied the effects of momentum smearing and shifting on the ΔE selection criteria, and assign an error of about 3.0% for this effect. Comparing data and Monte Carlo efficiencies for the m_{ES} requirement in the J/ψ control region, we assign a 3.0% error for the modeling of this requirement. We have compared the data and Monte Carlo efficiencies for the B vertex probability and the Fisher discriminant selection criteria. For the former, we assign a systematic error of 3.0% for the $B^+ \rightarrow K^+\ell^+\ell^-$ modes and 4.0% for the $B^0 \rightarrow K^{*0}\ell^+\ell^-$ modes. For the latter, we assign an error of 3.0% for all of the four modes. Furthermore, as a check that we understand our signal efficiencies, we have compared the yields in data and Monte Carlo events for the $B^+ \rightarrow J/\psi K^+$ and $B^0 \rightarrow J/\psi K^{*0}$ (with $K^{*0} \rightarrow K^+\pi^-$) channels. We have used the world average [9] branching fractions for $B^+ \rightarrow J/\psi K^+$ and $B^0 \rightarrow J/\psi K^{*0}$ and found agreement within

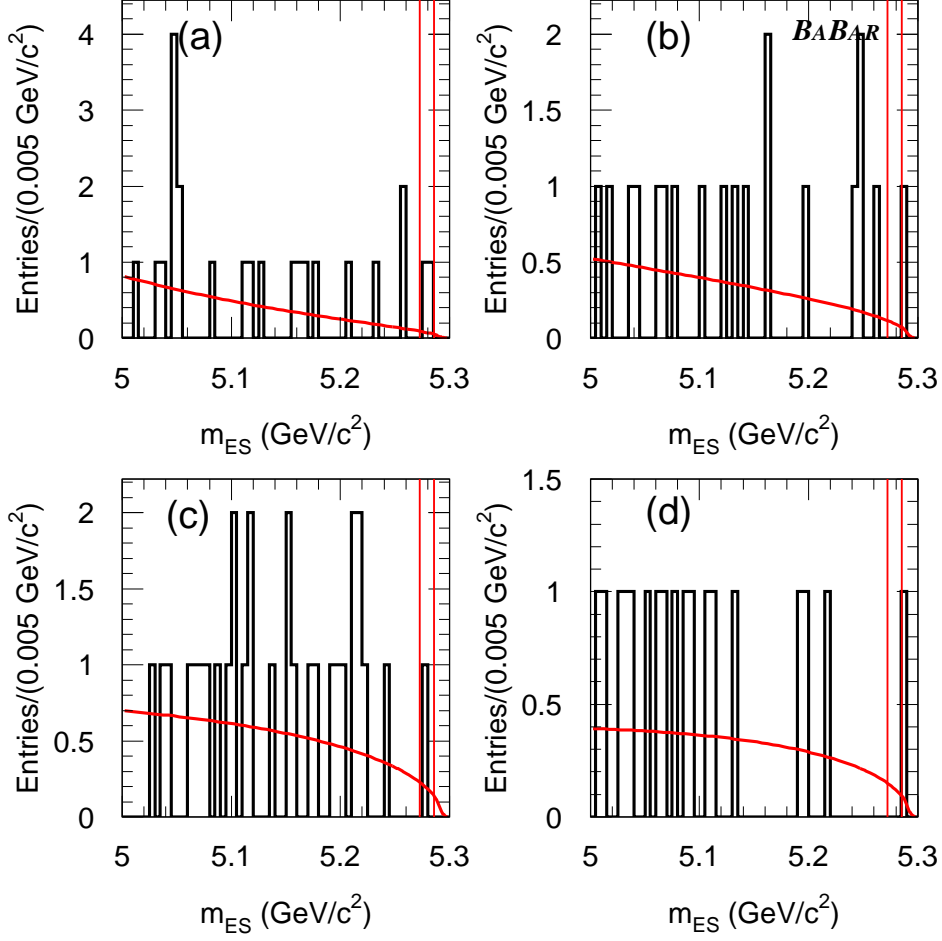


Figure 5: m_{ES} for data after all other event selection criteria are applied: (a) $B^+ \rightarrow K^+ e^+ e^-$, (b) $B^+ \rightarrow K^+ \mu^+ \mu^-$, (c) $B^0 \rightarrow K^{*0} e^+ e^-$, and (d) $B^0 \rightarrow K^{*0} \mu^+ \mu^-$. The shape of the fit (the ARGUS function) is obtained from the large statistics sample of fast parametrized Monte Carlo events. The lines indicate the signal region.

the statistical errors between the data and Monte Carlo samples.

8 Summary

We have searched for rare B decays $B \rightarrow K^{(*)} \ell^+ \ell^-$ in a sample of 3.7×10^6 $B\bar{B}$ events. We find no observable signal for any of the four modes considered, and set preliminary 90% C.L. upper limits on the branching fractions of

$$\begin{aligned} \mathcal{B}(B^+ \rightarrow K^+ e^+ e^-) &< 12.5 \times 10^{-6}, \\ \mathcal{B}(B^+ \rightarrow K^+ \mu^+ \mu^-) &< 8.3 \times 10^{-6}, \end{aligned}$$

Table 1: Signal efficiencies, systematic uncertainties (combining the uncertainties on the signal efficiencies and on the number of produced $\mathcal{T}(4S)$ mesons, as listed in Table 2), the number of observed events, the number of estimated background events, and upper limits on the branching fractions. In computing the upper limits we have assumed $\mathcal{B}(K^{*0} \rightarrow K^+\pi^-) = 2/3$.

| Mode | Efficiency (%) | Total systematic uncertainty (%) | Observed events | Bkgd. estimated from data | $\mathcal{B}/10^{-6}$ (90% C.L.) |
|------------------------------------|----------------|----------------------------------|-----------------|---------------------------|----------------------------------|
| $B^+ \rightarrow K^+e^+e^-$ | 13.1 | 11.7 | 2 | 0.20 | < 12.5 |
| $B^+ \rightarrow K^+\mu^+\mu^-$ | 8.6 | 12.3 | 0 | 0.25 | < 8.3 |
| $B^0 \rightarrow K^{*0}e^+e^-$ | 7.7 | 14.2 | 1 | 0.50 | < 24.1 |
| $B^0 \rightarrow K^{*0}\mu^+\mu^-$ | 4.5 | 14.8 | 0 | 0.33 | < 24.5 |

Table 2: Summary of the systematic uncertainties on the signal efficiencies and the number of produced $\mathcal{T}(4S)$ mesons as a percentage error on the branching fraction, \mathcal{B} . The total systematic error is the sum of the individual contributions added in quadrature.

| | $(\Delta\mathcal{B}/\mathcal{B})$ (%) | | | |
|--------------------------------------|---------------------------------------|-----------------|---------------|-------------------|
| | $Ke\bar{e}$ | $K\mu\bar{\mu}$ | $K^*e\bar{e}$ | $K^*\mu\bar{\mu}$ |
| Tracking efficiency | 7.5 | 7.5 | 10.0 | 10.0 |
| Lepton identification | 4.0 | 5.0 | 4.0 | 5.0 |
| Kaon identification | 3.0 | 3.0 | 3.0 | 3.0 |
| ΔE requirement efficiency | 2.0 | 2.5 | 3.3 | 1.5 |
| m_{ES} requirement efficiency | 3.0 | 3.0 | 3.0 | 3.0 |
| Vertex requirement efficiency | 3.0 | 3.0 | 4.0 | 4.0 |
| Fisher requirement efficiency | 3.0 | 3.0 | 3.0 | 3.0 |
| Number of produced $\mathcal{T}(4S)$ | 3.6 | 3.6 | 3.6 | 3.6 |
| MC signal statistics | 3.4 | 4.0 | 4.3 | 6.1 |
| Total systematic error | 11.7 | 12.3 | 14.2 | 14.8 |

$$\begin{aligned} \mathcal{B}(B^0 \rightarrow K^{*0}e^+e^-) &< 24.1 \times 10^{-6}, \\ \mathcal{B}(B^0 \rightarrow K^{*0}\mu^+\mu^-) &< 24.5 \times 10^{-6}. \end{aligned}$$

The limits for the $B^+ \rightarrow K^+\ell^+\ell^-$ modes are comparable to those set by other experiments, while those for $B^0 \rightarrow K^{*0}\ell^+\ell^-$ are less sensitive with this data sample. We plan to analyze substantially more data in the near future.

9 Acknowledgments

The authors thank JoAnne Hewett and Gudrun Hiller for their advice on theoretical issues related to the analysis.

We are grateful for the contributions of our PEP-II colleagues in achieving the excellent luminosity and machine conditions that have made this work possible. We acknowledge support from the Natural Sciences and Engineering Research Council (Canada), Institute of High Energy Physics (China), Commissariat à l’Energie Atomique and Institut National de Physique Nucléaire et de Physique des Particules (France), Bundesministerium für Bildung und Forschung (Germany), Istituto Nazionale di Fisica Nucleare (Italy), The Research Council of Norway, Ministry of Science and Technology of the Russian Federation, Particle Physics and Astronomy Research Council (United Kingdom), the Department of Energy (US), and the National Science Foundation (US). In addition, individual support has been received from the Swiss National Foundation, the A. P. Sloan Foundation, the Research Corporation, and the Alexander von Humboldt Foundation. The visiting groups wish to thank SLAC for the support and kind hospitality extended to them.

References

- [1] A. Ali, P. Ball, L.T. Handoki, and G. Hiller, *Phys. Rev. D* **61**, 074024 (2000).
- [2] G. Buchalla, G. Hiller, and G. Isidori, preprint hep-ph/0006136.
- [3] CDF Collaboration, T. Affolder *et al.*, *Phys. Rev. Lett.* **83**, 3378 (1999).
- [4] CLEO CONF 98-22, ICHEP98 1012 (1998).
- [5] ARGUS Collaboration, H. Albrecht *et al.*, *Z. Phys. C* **48**, 543 (1990).
- [6] BABAR Collaboration, B. Aubert *et al.*, “The first year of the BABAR experiment at PEP-II”, BABAR-CONF-00/17, submitted to the XXXth International Conference on High Energy Physics, Osaka, Japan.
- [7] G. C. Fox and S. Wolfram, *Phys. Rev. Lett.* **41**, 1581 (1978).
- [8] D. Lange and A. Ryd, “The EvtGen Event Generator Package”, presented at the International Conference on Computing in High Energy Physics, Chicago, 1998.
- [9] Particle Data Group, D. E. Groom *et al.*, *Eur. Phys. Jour. C* **15**, 1 (2000).
- [10] G. J. Feldman and R. D. Cousins, *Phys. Rev. D* **57**, 3873 (1998).